Axial Inlet Geometry Effects on the Flow Structures in a Cyclone Burner Related to the Combustion Performance of Biomass Particles

Pasymi[1,2], Yogi Wibisono Budhi[1] & Yazid Bindar[1,*]

[1]Department of Chemical Engineering, Faculty of Industrial Technology, Institut Teknologi Bandung, Jalan Ganesha No. 10 Bandung 40132, West Java, Indonesia
[2]Department of Chemical Engineering, Faculty of Industrial Technology, Bung Hatta University, Jalan Gajah Mada No. 19, Gunung Pangilun, Padang 25142, West Sumatera, Indonesia
*E-mail: ybybyb@fti.itb.ac.id

Abstract. Solid fuel combustion is always preceded by chemical decomposition. This process is largely determined by the flow structure and affected by the geometry and operating conditions of the combustion chamber. This study aimed to investigate the effect of relative axial inlet diameter ($D_{ai}//D_{bc}$) on the flow structure in the proposed cyclone burner. The flow structure was determined with the standard k-ε turbulent model using the Ansys-Fluent software. From the simulation results it was concluded that with all the axial inlet diameters used an integrated vortex formed in the center of the burner cylinder. The integrated vortex consisted of two vortices, namely a primary vortex and a secondary vortex. The primary vortex penetrated from the furnace box to the burner cylinder, while the secondary vortex was formed in the burner cylinder itself. There were two integration patterns from the primary vortex and the secondary vortex, namely a summation pattern and a multilayer pattern. The presence of a vortex in the center of the burner cylinder is allegedly responsible for an increase in the degree of mixing and pressure drop in that zone. The flow structure induced from the proposed burner had high symmetricity and was largely determined by the burner's axial inlet diameter.

Keywords: *axial inlet diameter; biomass particles; decomposition process; flow structure; k-ε turbulent model; pressure drop; turbulent intensity; vortex.*

1 Introduction

The design of a boiler furnace system, especially its burner design, is strongly influenced by the phase of fuel used. When using a liquid or gaseous fuel, the fuel can be directly burned in the boiler furnace. Meanwhile, when using a solid fuel, the fuel must be decomposed first in the burner before it can be burned completely in the boiler furnace [1]. This is why the design of a solid-fueled burner is more complex than that of gaseous and liquid burners. Although the

Received March 26th, 2018, Revised July 31st, 2018, Accepted for publication November 16th, 2018.
 ISSN: 2337-5779, DOI: 10.5614/j.eng.technol.sci.2018.50.5.7

design of coal burners has reached an established stage, it is not directly suitable for other solid fuels.

The design of a burner for solid fuel is determined largely by its physical and chemical characteristics, as stated by Baxter, *et al.* [2] and Momeni, *et al.* [3]. The physical and chemical characteristics of the biomass are much different from coal, therefore the geometrical design and operating conditions of a biomass burner need to be developed separately. The burner design proposed in this paper is intended for non-woody biomass fuel, i.e. *Miscanthus x Giganteus*. Its particles tend to have a higher surface area than coal due to their lower sphericity. It is relatively easy to flow because of its low density. Furthermore, it is relatively easy to decompose because of its high volatile content [4,5].

Fundamentally, solid fuel decomposition consists of body heating and volatile gas release. It involves many fields of science, such as fluid dynamics, heat transfer, thermodynamics and chemical kinetics [6]. Thermodynamically, the decomposition process is endothermic, so it requires a certain amount of heat. To meet the heat requirement of the decomposition process, some parts of the devolatilization gases are burned in the burner. Another potential heat source for the decomposition process is hot flue gas that comes from the boiler furnace.

Recirculation of hot flue gas into the burner can be done through the installation of a recycle flow pipe or through the formation of backflow patterns. In this study, the strategy chosen was the formation of backflow patterns, which can be created by involving the tangential or swirl flow in the burner. This backflow will carry hot flue gas from the boiler furnace to the internal burner and can maintain a high burner temperature. Thus, evaluation of this fluid dynamics characteristic can be used as a decomposition process indicator.

The formation of backflow patterns in a burner is influenced by the burner geometry and the operating conditions. According to Nemoda, *et al.* [7], the formation of backflow patterns in a burner is strongly influenced by the flow swirl number (Sn). Backflow patterns are only formed at high swirl numbers ($Sn > 2.48$). Meanwhile, Ziqiang, *et al.* [8] state that the backflow patterns in a burner are influenced by the tangential inlet orientation. They claim that a tangential inlet slope of 30° is the best angle to produce uniform and widespread backflow patterns.

Arnao, *et al.* [9] has succeeded in improving the performance of a sugar-cane bagasse swirl burner in Brazil by changing the geometry of the swirl generator. They claim that their design is able to increase fuel penetration and scattering in the furnace. Pasymi, *et al.* [10] numerically found that the initial tangential intensity (I_{it}), which is the ratio between the total momentum flux entering the

tangential inlet and the total momentum flux entering the burner cylinder, significantly affects the fluid dynamics characteristics inside the burner cylinder, especially at high initial tangential intensity.

Another fluid dynamics characteristic that can be evaluated as decomposition process indicator is turbulent intensity [11]. The turbulent intensity is associated with the degree of mixing: the higher the turbulent intensity, the higher the degree of mixing and vice versa. In turn the degree of mixing influences the mass diffusion and convective heat transfer coefficient. Moreover, the pressure drop is correlated to the burner operating cost. The higher the pressure drop, the greater the power required to drain the air and fuel from the boiler furnace, resulting in higher burner operating cost. This fluid dynamics characteristic can also be evaluated as a respone variable. Although the study of biomass burner design has been widely conducted, there are several aspects of this subject that still need to be investigated, whether related to the geometry or the operating conditions.

This study aimed to investigate the effect of the axial inlet diameter (D_{ai}) on the behaviors of fluid dynamics in the proposed burner. Evaluation of fluid dynamics behaviors was only done in the cylinder of the burner because the particle decomposition is expected to occur there. The information obtained from this study can be used as a consideration in developing the design of biomass burners.

2 Investigation Methodology

This research was conducted using a numerical simulation and the computational fluid dynamic (CFD) method. The CFD engine used was Ansys-Fluent. This method has several advantages, especially for the design and operation research goals, i.e. it can save research time and cost while still producing satisfactory results [12,13].

2.1 Computational Technique

The simulation of fluid dynamics in the burner started with drawing the geometry of the proposed burner. The geometry and dimensions of the proposed burner are given in Subsection 2.2. The second step was to mesh the burner geometry. The meshing type used was Cooper with hexagonal elements. The number of grid cells was about 1.200.000. The next step was to develop the discretization equation for each formed grid cell by integrating any differential equation present in the k-ε model. The differential equation system of the k-ε turbulence model is given in Subsection 2.3. The last step was to compute the discretization equation system by a numerical solver. The solver was worked

under steady state condition, simple schema of pressure-velocity coupling and default spatial discretization. The last two steps are available in the commercial Ansys-Fluent software.

2.2 Burner Geometry

The geometry of the proposed biomass burner consists of inlet and body sections. The inlet section is a cylindrical pipe embedded by an extended axial inlet and four tangential injections. The axial inlet is a cylinder with diameter D_{ai} and length L_{ai} and it is concentric with the cylinder of the inlet section. The tangential injection is a rectangular duct with thickness *t,* width ℓ and length L_{ti}.

The four tangential injections are mounted symmetrically on the cylinder of the inlet section. Based on Ziqiang, *et al.* [9], the tangential injection orientation angle used in this study was 30°. Meanwhile, the body section of the burner is also a cylinder, with diameter Dbc and length Lbc. The geometry and dimensions of the burner are shown in Figure 1.

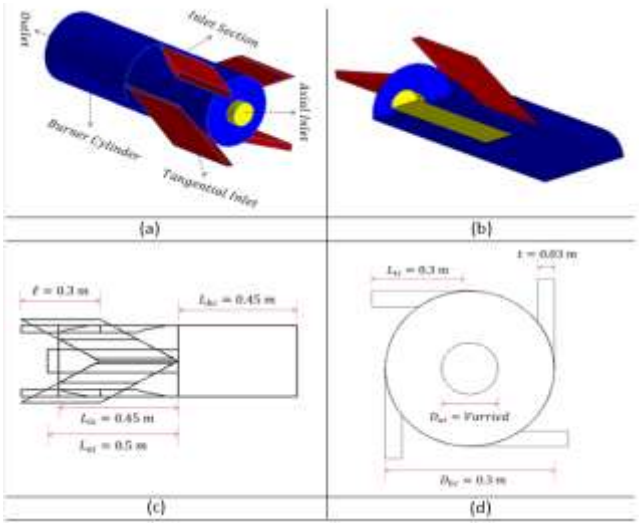

Figure 1 The proposed burner's geometry and dimensions: (a) complete geometry, (b) longitudinal slice geometry, (c) longitudinal dimensions, and (d) cross section dimensions.

For modeling purposes, the simulated burner is equipped with a rectangular box at the end of the burner cylinder, which is 2 m in length and width, and 3 m in height. At the top of the box, there is a rectangular area for the flue gas outlet, which is 2 m in length and 0.5 m in width.

2.3 Fluid Dynamics Modeling Formulation

Fluid dynamics modeling in this research was conducted using mass and momentum turbulent conservation equations, also known as Reynolds Average Navier-Stokes (RANS) equations. Meanwhile, the strategy or model used to solve the equation system was the standard k-ε turbulent model.

Although derived with isotropic turbulent assumption, the standard k-ε turbulent model works well for low swirl flow, as stated by Pasymi, *et al.* [11], Bindar, [14] and Vazquez [15]. As found in [16], the formulations of the fluid dynamics equations system according to the standard k-ε turbulent model are expressed in Eqs. (1) to (6). The constitutive equations needed to solve the equation system are given in Eqs. (7) to (9).

$$\frac{\partial \rho}{\partial t} = \sum_{j=x}^{y,z} \left(\frac{\partial \rho \bar{u}_j}{\partial j} \right) \tag{1}$$

$$\frac{\partial \rho \bar{u}_x}{\partial t} + \sum_{j=x}^{y,z} \left(u_j \frac{\partial \rho \bar{u}_x}{\partial j} \right) = -\frac{\partial \bar{p}}{\partial x} + \sum_{j=x}^{y,z} \frac{\partial}{\partial j} \left[\mu_{\text{eff}} \frac{\partial \bar{u}_x}{\partial j} \right] + \rho g_x \tag{2}$$

$$\frac{\partial \rho \bar{u}_y}{\partial t} + \sum_{j=x}^{y,z} \left(u_j \frac{\partial \rho \bar{u}_y}{\partial j} \right) = -\frac{\partial \bar{p}}{\partial y} + \sum_{j=x}^{y,z} \frac{\partial}{\partial j} \left[\mu_{\text{eff}} \frac{\partial \bar{u}_y}{\partial j} \right] + \rho g_y \tag{3}$$

$$\frac{\partial \rho \bar{u}_z}{\partial t} + \sum_{j=x}^{y,z} \left(u_j \frac{\partial \rho \bar{u}_z}{\partial j} \right) = -\frac{\partial \bar{p}}{\partial z} + \sum_{j=x}^{y,z} \frac{\partial}{\partial j} \left[\mu_{\text{eff}} \frac{\partial \bar{u}_z}{\partial j} \right] + \rho g_z \tag{4}$$

$$\rho \frac{\partial k}{\partial t} + \sum_{j=x}^{y,z} \rho \bar{u}_j \frac{\partial k}{\partial j} = \sum_{j=x}^{y,z} \frac{\partial}{\partial j} \left[\frac{\mu_{\text{eff}}}{\sigma_{\text{k}}} \frac{\partial k}{\partial j} \right] + G_{\text{k}} - \rho \varepsilon \tag{5}$$

$$\rho \frac{\partial \varepsilon}{\partial t} + \sum_{j=x}^{y,z} \rho \bar{u}_j \frac{\partial \varepsilon}{\partial j} = \sum_{j=x}^{y,z} \frac{\partial}{\partial j} \left[\frac{\mu_{\text{eff}}}{\sigma_{\varepsilon}} \frac{\partial \varepsilon}{\partial j} \right] + C_{\varepsilon 1} \frac{\varepsilon}{k} G_k - C_{\varepsilon 2} \rho \frac{\varepsilon^2}{k} \tag{6}$$

$$G_k = 2\mu_t \left[\left(\frac{\partial \bar{u}_x}{\partial x} \right)^2 + \left(\frac{\partial \bar{u}_y}{\partial y} \right)^2 + \left(\frac{\partial \bar{u}_z}{\partial z} \right)^2 \right] + \mu_t \left(\frac{\partial \bar{u}_x}{\partial y} + \frac{\partial \bar{u}_y}{\partial x} \right)^2$$
$$+ \mu_t \left(\frac{\partial \bar{u}_x}{\partial z} + \frac{\partial \bar{u}_z}{\partial x} \right)^2 + \mu_t \left(\frac{\partial \bar{u}_y}{\partial z} + \frac{\partial \bar{u}_z}{\partial y} \right)^2 \tag{7}$$

$$\mu_{eff} = \mu + \mu_t \tag{8}$$

$$\mu_t = C_\mu \rho \left({}^{k^2}/_{\varepsilon} \right) \tag{9}$$

C_μ, $C_{\varepsilon 1}$, $C_{\varepsilon 2}$, σ_{k} and σ_ε are the empirical constants of these equations. The value of each of the empirical constants is 0.09 for C_μ, 1.0 for σ_{k}, 1.3 for σ_{k}, 1.44 for $C_{\varepsilon 1}$ and 1.92 for $C_{\varepsilon 2}$. The simultaneous solution of the equation system above will produce 6 dependent variable values, namely; $\bar{p}$, k, ε, $\bar{u}_x$, $\bar{u}_y$ and $\bar{u}_z$ and can be expressed in various response variables.

2.4 Research Variables and Parameters

As stated in the previous section, the independent variable used in this study is the axial inlet diameter (D_{ai}). The variation of axial inlet diameter was expressed as the diameter ratio of axial inlet and burner cylinder (D_{ai}/D_{bc}). There were 6 different D_{ai}/D_{bc} values used, i.e. 0.20, 0.33, 0.40, 0.50, 0.60 and 0.80.

All simulations were performed under constant initial tangential intensity (I_{it}) and flow Reynolds number (N_{Re}). The initial tangential intensity and the Reynolds number values used were 3.7 and 69,000, respectively. These low I_{it} and N_{Re} were chosen in view of the low density of the biomass particle. The initial tangential intensity was calculated using Eq. (10) and the flow Reynolds number was found through Eq. (11).

$$I_{it} = \left(\frac{\dot{m}_t}{\dot{m}_T}\right)^2 \left(\frac{A_T}{A_t}\right)^2 \tag{10}$$

$$N_{Re} = (\rho D_{bc} \bar{u}_{av})/\mu \tag{11}$$

The response variables used were extracted from the dependent variables resulted from the simulation. They were: flow structure, pressure drop and degree of mixing. The flow structure was represented by recirculation flow patterns and velocity profiles, while the pressure drop was represented by the static pressure profile. The degree of mixing was represented by the turbulent intensity and was determined through Eq. (12):

$$I = \sqrt{\frac{(2/3)\,k}{(\bar{u}_x{}^2 + \bar{u}_y{}^2 + \bar{u}_z{}^2)}} \tag{12}$$

3 Results and Discussion

3.1 Flow Structure

The simulation results showed that the flow structure in the burner cylinder consists of recirculation and non-recirculation flows, as shown in Figure 2. The recirculation flows occur at the center of the burner cylinder, while non-recirculation flows occur in the area near the burner wall. In Figure 2(a), the axial velocity distribution of the velocity vector in longitudinal fields, namely the zx and zy planes of the burner, is presented. The recirculation flow is represented by the axial velocity vector leading to the left in the center of the burner cylinder. Meanwhile, in Figure 2(b) the distribution of axial velocity in several cross sections along the burner cylinder is shown. The recirculation flow is represented by purple and blue colors of the axial velocity vector at the center of each cross section field.

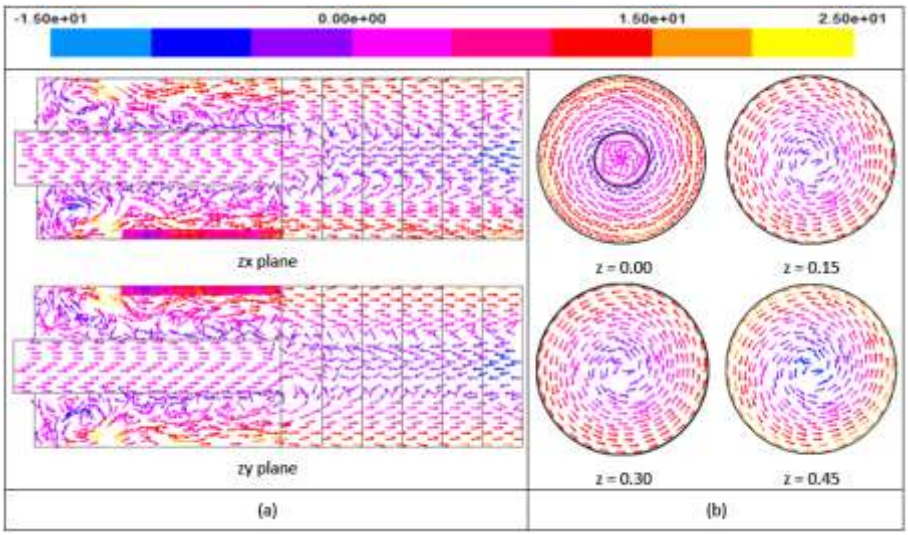

Figure 2 Velocity vectors colored by axial velocity (m/s) for Dai/Dbc = 0.33; (a) in longitudinal field and (b) in cross section. Colors indicate velocity magnitude.

The flow pathlines showed that the recirculation flow in the burner cylinder forms an integrated vortex that resembles a tornado tail, as shown in Figure 3-5. The integrated vortex consists of two vortices, namely a primary vortex and a secondary vortex. The primary vortex is a vortex that extends from the furnace box to the burner cylinder, as shown in Figure 3. The secondary vortex is a vortex that forms in the burner cylinder itself, as shown in Figure 4. There are two kinds of secondary vortex flow orientations: one is unidirectional to the primary vortex, see Figures 4(a) and 4(b), while the other is in the direction opposite to the primary vortex, see Figures 4(c)-4(f).

The penetration length and orientation of both vortices was determined by the relative diameter of axial inlet (D_{ai}/D_{bc}). The smaller the D_{ai}/D_{bc} value, the longer the backflow penetration of the primary vortex that was formed and vice versa. The unidirectional secondary vortex orientation tends to form at lower D_{ai}/D_{bc} values.

The assimilation of the primary vortex to the secondary vortex has two patterns, namely a summation pattern and a multilayer pattern. In the summation pattern, the total penetration length of the recirculation flows is the sum of the primary and the secondary vortex length, as depicted by Figure 5(a). On the other hand, in the multilayer pattern, the secondary vortex enclosed the primary vortex, as illustrated by Figure 5(b). The assimilation pattern of the vortex is also determined by the relative diameter of axial inlet (D_{ai}/D_{bc}). In this simulation,

the summation pattern was formed at D_{ai}/D_{bc} of 0.20 and 0.33, and tended to have longer vortex penetration lengths. Meanwhile the multilayer patterns occured at D_{ai}/D_{bc} values of 0.4 to 0.80 and tended to have larger vortex diameters.

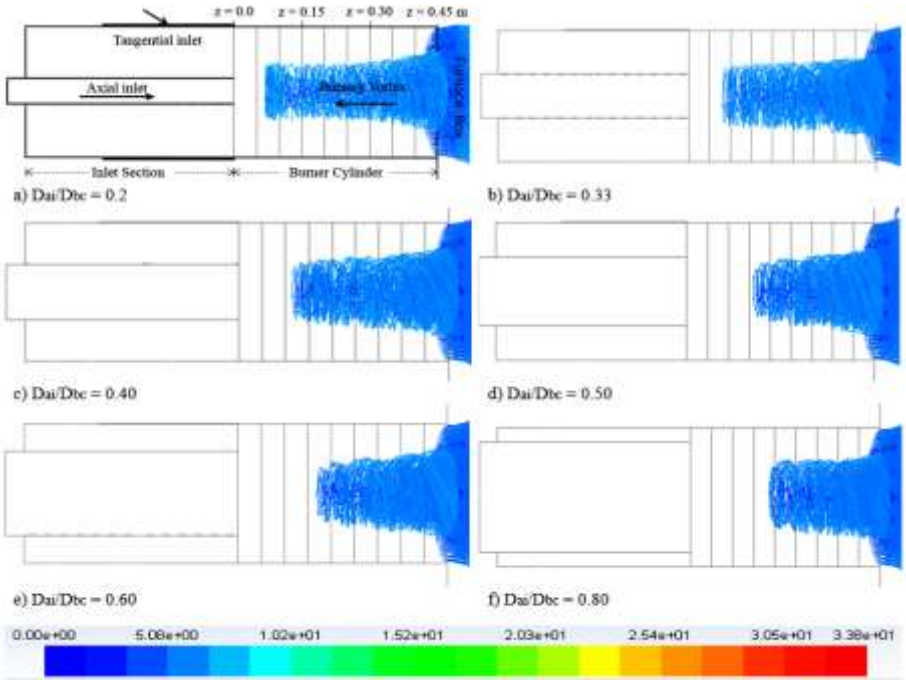

Figure 3 The tornado-tail like flow patterns (primary vortex) for several D_{ai}/D_{bc} values. Colors indicate velocity magnitude.

This study described how the axial inlet diameter affects the recirculation flow pattern in the burner cylinder and contributed in selecting a proper burner axial inlet diameter. According to Nemoda, *et al.* [8] and Al-Abdeli & Masri [17], the recirculation flow will bring hot flue gas from the furnace into the burner to keep the burner temperature high. That is why the recirculation flow is highly responsible for the flame stability in the burner.

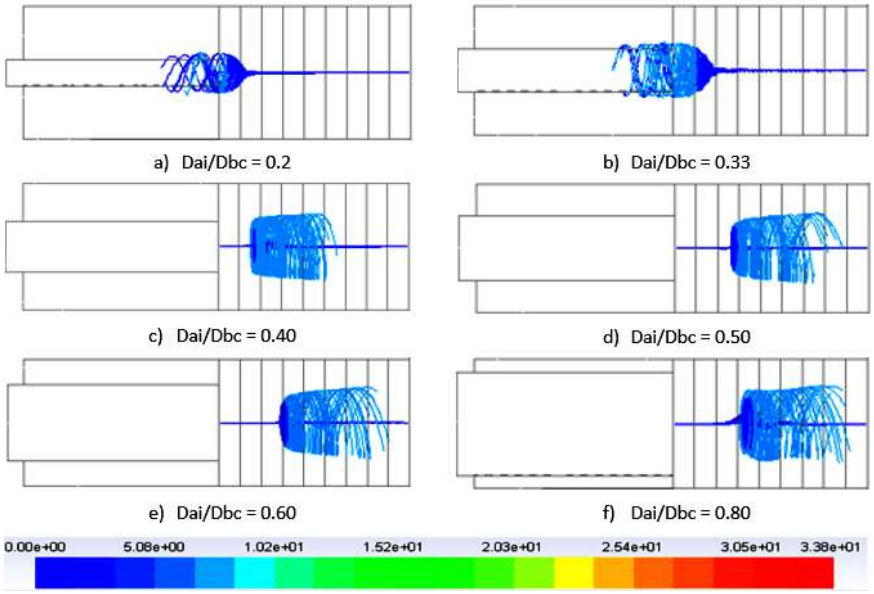

Figure 4 The secondary vortex patterns in the center of the burner cylinder for several D_{ai}/D_{bc} values. Colors indicate velocity magnitude.

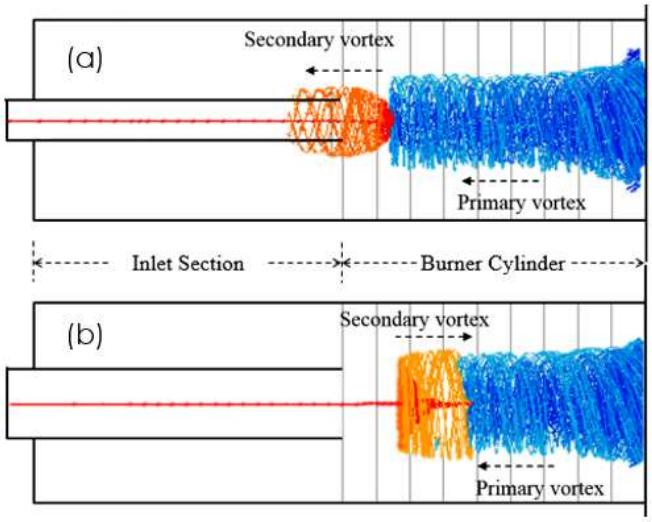

Figure 5 Schematic of assimilation patterns from the primary vortex and secondary vortex: (a) summation pattern and (b) multilayer pattern.

3.2 Turbulent Intensity

Referring to Nag [7], a high degree of mixing is needed in operating a burner. The mixing will intensify the contact between air and fuel to actualize the combustion process. Furthermore, the degree of mixing will also affect the fluid residence time [18]. The degree of mixing is greatly affected by the geometry and operating conditions of the chamber. The following discussion describes the effect of the axial inlet diameter on the degree of mixing in the burner cylinder. The degree of mixing is represented by the turbulent intensity.

The radial and axial profiles of the turbulent intensity in the burner cylinder are shown in Figure 6. Radially, the closer to the cylinder center, the higher the turbulent intensity, as can be seen in Figure 3(a) and 3(b). The value and position of the turbulent intensity peak in the burner centerline is determined by D_{ai}/D_{bc}. The higher D_{ai}/D_{bc}, the higher the turbulent intensity and the closer turbulent intensity peak to the burner outlet, as shown in Figure 6(c). The profile of turbulent intensity in the burner is likely correlated to the vortex structure. The highest turbulent intensity was obtained at Dai/Dbc = 0.8, where the value of turbulent intensity was ± 2.78% and the peak position of the turbulent intensity was at ± 0.26 m from the burner outlet.

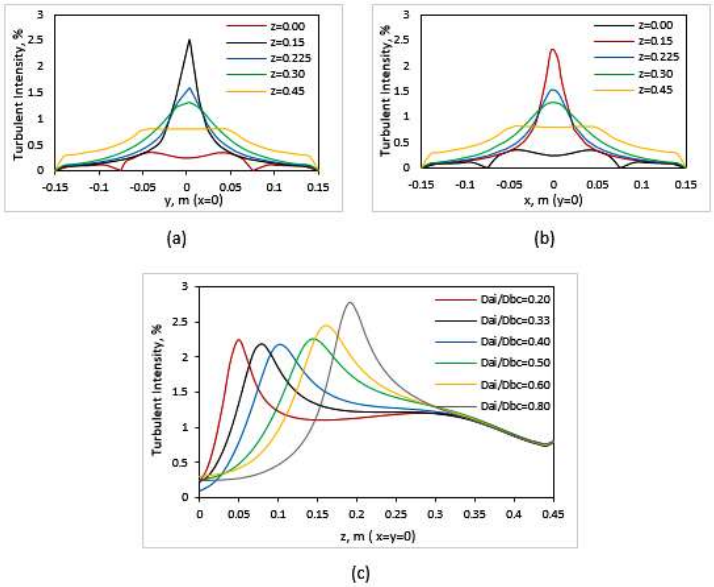

Figure 6 Turbulent intensity profile in the burner cylinder: (a) radially, at several z positions in the zy plane for D_{ai}/D_{bc} = 0.33, (b) radially, at several z positions in the zx plane for D_{ai}/D_{bc} = 0.33, and (c) at the centerline of the burner cylinder for several D_{ai}/D_{bc} values.

Meanwhile, the lowest one was found at D_{ai}/D_{bc} = 0.4. The value of turbulent intensity was ± 2.18% and the peak position of the turbulent intensity was at ± 0.35 m from the burner outlet.

3.3 Pressure Drop

In this section, the pressure drop in the burner cylinder is represented by the radial and axial profile of static pressure. Radially, the static pressure was greater toward the wall, as shown in Figure 7(a) and 7(b). This is because the closer to the wall, the higher the friction loss and the greater the flow resistance or static pressure. Axially, in the near wall zone, the static pressure in the burner cylinder decreased toward the outlet. In the central zone of the burner cylinder the static pressure increased toward the outlet, as shown in Figure 7(c) and 7(d). The presence of recirculation flow at the center of the burner cylinder is allegedly responsible for an increase in static pressure in that zone.

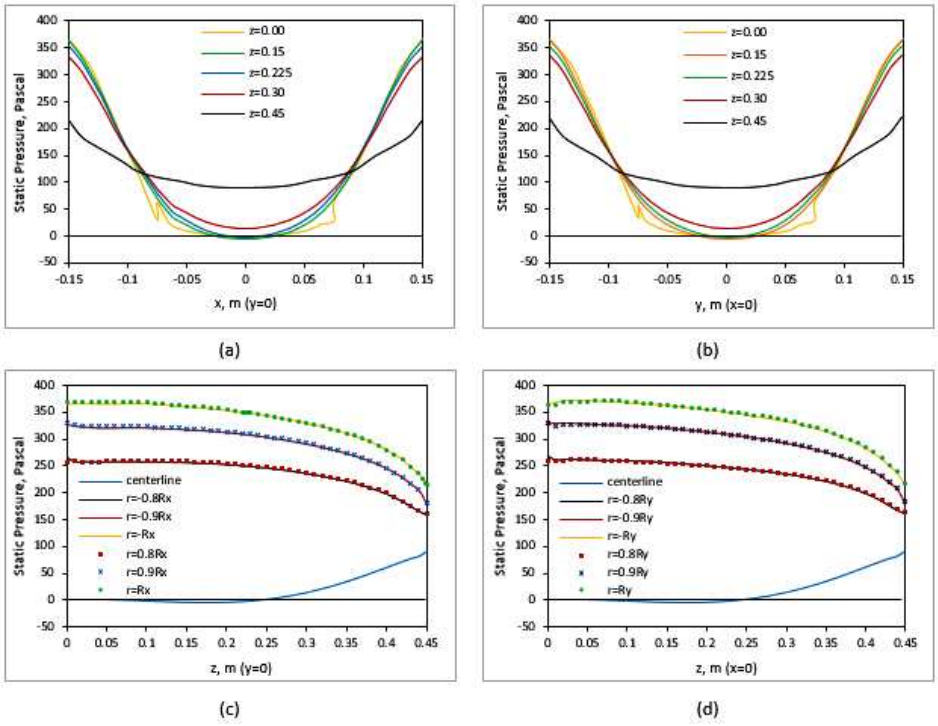

Figure 7 Profile of the static pressure along the burner for D_{ai}/D_{bc} = 0.33: (a) radially, for several z positions in the zx plane, (b) radially, for several z positions in the zy plane, (c) axially, for several r positions in the zx plane and (d) axially, for several r positions in the zy plane.

4 Conclusion

A fluid dynamics simulation was conducted to study the effect of axial inlet diameter on the flow structure in a burner cylinder using the standard k-ε turbulent model. With all axial inlet diameters used, an integrated vortex formed at the center of the burner cylinder. The integrated vortex consisted of two vortices, namely a primary vortex and a secondary vortex. The primary vortex penetrated from the furnace box to the burner cylinder, while the secondary vortex was formed in the burner cylinder itself.

There were two integration patterns from the primary vortex and the secondary vortex, namely a summation pattern and a multilayer pattern. In the summation pattern, the total penetration length of the integrated vortex was the sum of both vortices penetration lengths. Meanwhile, in the multilayer pattern the secondary vortex enclosed the primary vortex, so that the integrated vortex diameter became larger. The presence of the vortex in the center of the burner cylinder is allegedly responsible for an increase in the degree of mixing and pressure drop in that zone.

Based on the profiles of velocity, pressure drop and turbulent intensity obtained from the simulation, it can be concluded that the flow structure in the burner cylinder of the proposed burner has a high symmetricity. The flow structure, including the vortex pattern in the burner is largely determined by the relative diameter of axial inlet (D_{ai}/D_{bc}). How the flow structure affects the biomass burner's design still needs deeper study.

Acknowledgement

Our thanks go to the expertise group research directorate of ITB for the funding support provided to the implementation of this research through P3MI scheme.

Nomenclature

Roman Letters

A	= surface area	$\bar{P}$	= average pressure
c	= specific heat capacity	$\bar{u}_x$	= average velocity of x component
$\dot{m}$	= mass flow rate	$\bar{u}_y$	= average velocity of y component
k	= turbulent kinetic energy	$\bar{u}_z$	= average velocity of z component
I	= turbulent intensity	C_μ	= empirical constant of μ_t
h	= convective heat transfer coefficient	$C_{\varepsilon 1}$	= empirical constant of ε
g	= acceleration gravity	$C_{\varepsilon 2}$	= empirical constant of ε

Greek Symbols

ε	= dissipation rate of k	ρ	= density
μ	= molecular viscosity	λ	= thermal conductivity
μ_t	= turbulent viscosity	σ_k	= empirical constant of k
μ_{eff}	= effective viscosity	σ_ε	= empirical constant of ε

References

[1] Li, J., Paul, M.C., Younger, P.L., Watson, I., Hossain, M. & Welch, S., *Combustion Modelling of Pulverized Biomass Particles at High Temperatures*, Energy Procedia, **66**, pp. 273-276, 2015.

[2] Baxter, L., Ip, L., Lu, H. & Tree, D., *Distinguishing Biomass Combustion Characteristics and Their Implications for Sustainable Energy*, Proc. of 5th Asia Pacific Conference on Combustion, University of Adelaide, Australia, pp. 469-473, 2005.

[3] Momeni, M., Yin, C., Kær, S.K., Hansen, T.B., Jensen, P.A. & Glarborg, P., *Experimental Study on Effects of Particle Shape and Operating Conditions on Combustion Characteristics of Single Biomass Particles*, Energy & Fuels, **27**, pp. 507-514, 2013.

[4] Vassilev, S.V., Vassileva, C.G. & Vassilev, V.S., *Advantages and Disadvantages of Composition and Properties of Biomass in Comparison with Coal: An Overview*, Fuel, **158**, pp. 330-350, 2015.

[5] Baxter, X.C., Darvell, L.I., Jones, J.M., Barraclough, T., Yates, N.E. & Shield, I., *Miscanthus Combustion Properties and Variations with Miscanthus Agronomy*, Fuel, **117**, pp. 851-869, 2014.

[6] Kops, S.M.B. & Malte, P.C., *Simulation and Modeling of Wood Dust Combustion in Cyclone Burners*, Final Technical Report (1-49), University of Washington, Washington DC, United States, 2004.

[7] Nemoda, S., Bakic, V., Oka, S., Zivkovic, G. & Crnomarkavic, N., *Experimental and Numerical Investigation of Gaseous Fuel Combustion in Swirl Chamber*, International Journal of Heat and Mass Transfer, **48**, pp. 4623-4632, 2005.

[8] Ziqiang, L.V., Guangqiang, L. & Yingjie, L., *Optimization Study on Bias Angle of a Swirl Burner with Tangential Inlet Air*, International Journal of Smart Home, **10**, pp. 171-180, 2016.

[9] Arnao, J.H.S., Ferreira, D.J.O., Santos, C.G., Alvarez, J.E., Rangel, L.P. & Park, S.W., *The Influence of Swirl Burner Geometry on the Sugar-Cane Bagasse Injection and Burning*, International Journal of Mechanical, Aerospace, Industrial, Mechatronic and Manufacturing Engineering, **9**, pp. 798-801, 2015.

[10] Pasymi, Budhi, Y.W. & Bindar, Y., *Effect of Initial Tangential Intensity on the Fluid Dynamic Characteristics in Tangential Burner*, MATEC Web of Conferences, **101**, pp. 1-6, 2017.
[11] Nag, P.K., *Power Plant Engineering, Second Edition*, McGraw Hill Company, Singapore, 2002.
[12] Xia, B. & Sun, D.W., *Applications of Computational Fluid Dynamics (CFD) in the Food Industry*, Journal of Computers and Electronics in Agriculture, **34**, pp. 5-24, 2002.
[13] Pragati, K. & Sharma, H.K., *Concept of Computational Fluid Dynamics (CFD) and its Applications in Food Processing Equipment Design*, Journal of Food Processing and Technology, **3**, pp. 1-7, 2013.
[14] Bindar, Y., *Geometry Effect Investigation on a Conical Chamber with Porous Media Boundary Condition Using Computational Fluid Dynamic (CFD) Technique*, J. Eng. Technol. Sci. (formerly as ITB J. Eng. Sci.), **41**, pp. 97-110, 2009.
[15] Vazquez, J.A.R., *A Computational Fluid Dynamics Investigation of Turbulent Swirling Burners*, PhD Thesis, University of Zaragoza, Spain, 2012.
[16] Bindar, Y., *Computation Engineering on Multi-Dimensional Turbulent Flows (in Indonesian Language), First Edition*, ITB Press, Bandung, 2017.
[17] Al-Abdeli Y.M. & Masri, A.R., *Review of Laboratory Swirl Burners and Experiments for Model Validation*, Journal of Experimental Thermal and Fluid Science, **69**, pp. 178-196, 2015.
[18] Ahsan, M. & Hussain, A., *Computational Fluid Dynamics (CFD) Simulation and Comparison for Different Numbers of Baffles to Reduce Concentration Polarization Effects in Membrane Tubes*, J. Eng. Technol. Sci., **49**(1), pp. 114-131, 2017.